Structure and Defects in Fully Syndiotactic Polypropylene

Andrew J. Lovinger,* Bernard Lotz,[1] Don D. Davis, and F. J. Padden, Jr.

AT&T Bell Laboratories, Murray Hill, New Jersey 07974

Received January 28, 1993; Revised Manuscript Received April 1, 1993

ABSTRACT: We have studied the structure and defects of fully syndiotactic polypropylene [sPP] in its dominant $(t_2g_2)_2$ phase using X-ray and electron diffraction and molecular modeling. In agreement with our previous proposal from much less syndioperfect sPP (77%), we find the chains to pack in a fully antichiral cell along *both* the *a* and *b* axes, which is thus doubled from its currently accepted dimensions. Cell parameters are a = 1.45 nm, b = 1.12 nm, c = 0.74 nm, and space group *Ibca*. Crystallization at temperatures below *ca.* 130 °C causes incorporation of packing defects along the *b* axis, which we have simulated using molecular modeling. At high crystallization temperatures, the defects consist of individual rows of chains displaced by *b*/4 and identified by narrow streaks superimposed upon sharp *h*20 spots in electron-diffraction patterns from tilted crystals. At lower crystallization temperatures, entire groups of such chains are displaced by *b*/4, forming discrete domains and leading to streaking of the individual *h*20 spots. No evidence for large-scale row or point vacancies is found. In addition, we find evidence for new intermolecular packing defects along the chain direction, which may arise from conformational defects and may involve small-scale (*ca.* 5–10% of *c*) axial displacements of the macromolecules.

Introduction

Contrary to isotactic polypropylene, which is one of the most widely used and studied polymers, syndiotactic polypropylene has received very little attention. This is primarily a result of the poor syndiospecificity of the earlier vanadium-based catalysts[2] and the consequent deterioration of the properties of the resulting polymer. However, in the last few years new metallocene catalysts based on Zr and Hf have been developed,[3] which allow very high syndiospecificity, purity, and yields. As a result, the properties of these new syndiotactic polypropylenes have been greatly improved and are now competitive with those of the isotactic isomer.

A number of alternative crystal structures have been proposed for syndiotactic polypropylene (sPP) in its dominant $(t_2g_2)_2$ conformation. The earliest one[4,5] has the molecules packed in a *C*-centered orthorhombic unit cell with a = 1.45 nm, b = 0.56 nm, and c = 0.74 nm, as depicted in Figure 1a (Cell I). More recently, we provided evidence for an alternative unit cell[6-8] (Cell II) having the same dimensions as Cell I but with all the molecules placed on the *ac* faces rather than *C*-centered (see Figure 1b). We also tentatively proposed[6] the possibility that the true unit cell may in fact be more complex, *i.e.*, *doubled* along the *b* axis and corresponding to an *Ibca* space group (this is depicted as Cell III in Figure 1c).

As we discussed at that time, these three possible unit cells result directly from the *chirality* of their constituent chains. This is shown schematically in Figure 2, which depicts in bold the bottom contact surfaces of a right- and a left-handed chain (**R** and **L**, respectively) as they deposit on the top contact surfaces of molecules on the *bc* plane. If adjacent molecules on the substrate are right-handed (R), then the only way that chain **R** can regularly crystallize (i.e., without steric conflict) is *in between* them; thus the *C*-centered packing (Cell I)[4,5] *requires* that all chains be of the *same* hand (isochiral). On the other hand, a left-handed chain (**L** in Figure 2) can also crystallize in a regular manner on the same substrate but *only directly on top* of a right-handed helix, using a *c*/2 axial shift. Therefore, the alternative model (Cell II) requires antichiral packing along its *a* axis. Our tentative suggestion of Cell III applies if the chains on the *substrate* also alternate in hand (as seen on the left side of Figure 2); this leads to doubling of the *b* axis and implies *fully antichiral* packing along *both* axes.

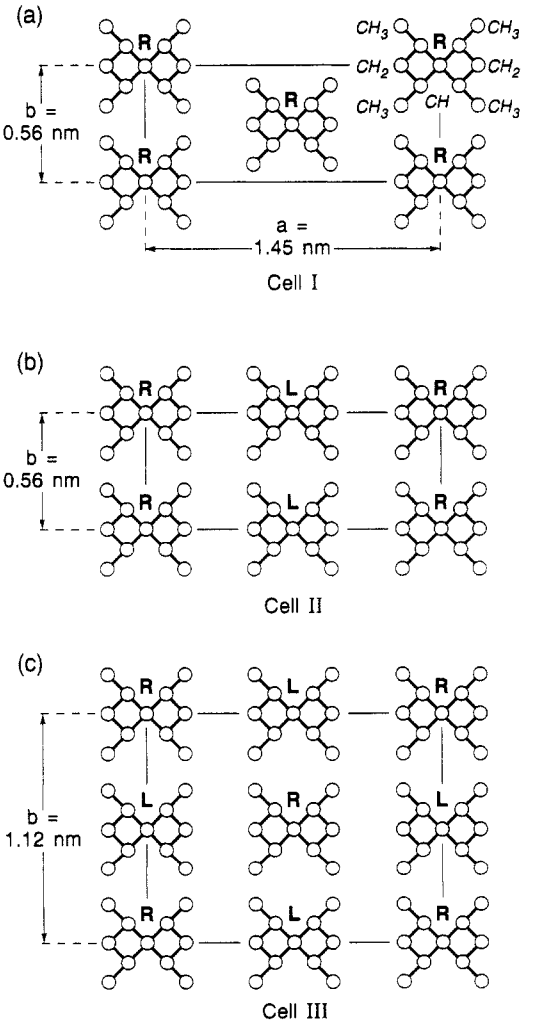

Figure 1. Proposed unit cells for the stable $(t_2g_2)_2$ form of sPP, shown in the *c* axis projection. (a) Fully isochiral, *C*-centered Cell I. (b) Primitive Cell II with antichiral packing of chains along the *a* axis. (c) Fully antichiral, body-centered Cell III. Right- and left-handed helical molecules are identified by **R** and **L**, respectively.

0024-9297/93/2226-3494$04.00/0

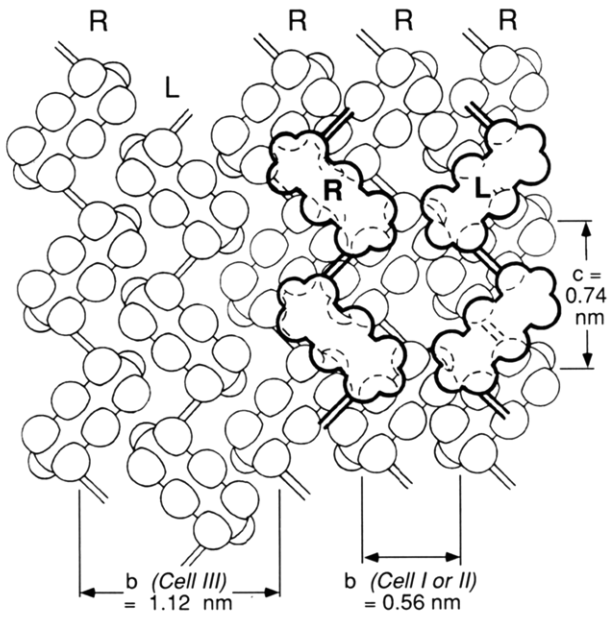

Figure 2. Schematic diagram showing the origins of isochiral *vs* antichiral packing in sPP (after ref 7). The top surfaces of chains on a *bc* substrate are shown with light lines, incorporating both antichiral (RLR) and isochiral (RRR) molecular packings. Superimposed with heavy lines are the contact (*i.e.*, bottom) surfaces of a right-handed (**R**) and a left-handed (**L**) helix crystallizing on this substrate. It is seen that, for steric reasons, a right-handed molecule can deposit only in between a pair of right-handed substrate helices (isochirally), whereas a left-handed molecule can do so only directly on top of a right-handed one (antichirally). As seen on the left half, only the antichiral deposition is possible for a Cell III substrate.

In this study, we demonstrate that the correct general structure is in fact this doubled Cell III and that other diffraction patterns (at lower temperatures) represent kinetically induced departures from it. We do this on the basis of the availability of new, highly syndiotactic samples (whose racemic-triad content exceeds 99%); in contrast, previously examined specimens throughout the literature had syndiotacticities on the order of only 60–77% (see our discussion in ref 7). Moreover, we also use molecular modeling to study the detailed nature of the packing defects that we had discovered earlier.[6,8]

Experimental Section

The sPP sample studied here was kindly provided by Dr. T. Simonazzi of Himont, Novara, Italy; it had been synthesized utilizing the highly syndiospecific method of Ewen *et al.*[3] High-resolution ^{13}C NMR spectroscopy showed >99% racemic triads. Thin films cast from xylene solution were melted and recrystallized under controlled conditions on freshly cleaved mica, following which they wer Pt-shadowed, C-coated, and otherwise processed for transmission electron microscopy and diffraction in the usual manner. Electron-diffraction patterns were obtained from diferent zones at 100 kV in a JEOL 100-CX transmission electron microscope. Thicker films and bulk samples were examined by X-ray diffraction in the reflection mode using a Rigaku diffractometer with Ni-filtered Cu Kα radiation at a scan rate of 0.5° 2θ/min. Optical diffractograms were obtained from model lattices that included defects, using a He–Ne laser on an optical bench under appropriate collimation and magnification. Molecular modeling and simulations of electron- and X-ray-diffraction patterns were conducted on a Silicon Graphics Computer System using the CERIUS program from Molecular Simulations Inc.

Results and Discussion

a. Single-Crystal Structure. The operative differences between Cell I, on the one hand, and Cells II and III, on the other, are manifested most clearly in the $h10$ layer (which becomes the $h20$ layer in Cell III). As can be deduced from Figure 1, on this layer Cell I has systematic absences for $h = 2n$, while Cells II and III have the opposite. The electron-diffraction patterns from specimens crystallized at the highest temperatures, *i.e.*, 130–145 °C (see Figure 3a,b) show a very prominent 010 reflection and total absence of the 110 (we should note that this 010 reflection for Cells I and II would be identified as 020 for Cell III because of the doubled *b* axis). This demonstrates that the packing of Cell I is absent in single crystals of the new, fully syndiotactic polypropylene.

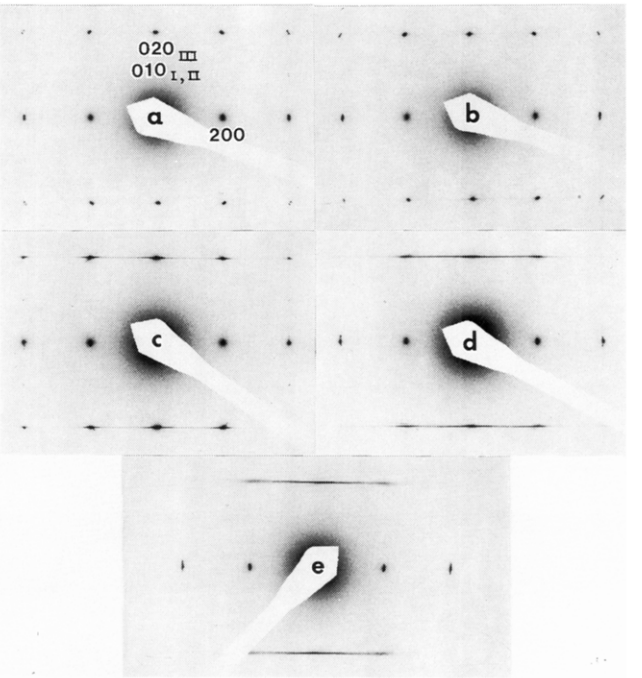

Figure 3. Electron-diffraction patterns of fully syndiotactic polypropylene single crystals grown isothermally at (a) 145, (b) 130, (c) 120, (d) 110, and (e) 100 °C. The electron beam is directed along [001], *i.e.*, normal to the lamellar crystals.

However, differentiation between Cells II and III cannot be made simply on the basis of these $hk0$ diffraction patterns; it will be made from tilted specimens later in this paper. First, however, we should observe the structural disorder at lower crystallization temperatures, evidenced through the streak along $h10$ in Figure 3c-e. This indicates statistical departures from regular antichiral packing along the *a* axis, as discussed in detail in ref 6. These interchain placement defects are associated with the rapidity of crystallization at lower temperatures, whereas slow growth at the higher temperatures yields essentially perfect antichiral packing. All of these findings from fully syndiotactic polypropylene are in agreement with our previous results from the stereochemically much more disordered sPP samples, with the difference that equivalent behavior is observed here at temperatures *ca.* 30–40 °C higher than in the previous samples. We attribute this increase to the much greater intrachain regularity of the new samples.

To determine whether the alternation in hand extends also to packing along the *b* axis (Cell III) or occurs only along the *a* axis (Cell II), we performed electron diffraction on specimens tilted about these two axes, as seen in Figure 4. Specimens crystallized at 100 °C show diffuse streaks along $h11$ in reciprocal space when tilted by 57° about the *a* axis (see Figure 4b). These streaks were the ones that we had also observed in our previous, more stereochemically defective samples (Figure 4b in ref 6) and had led

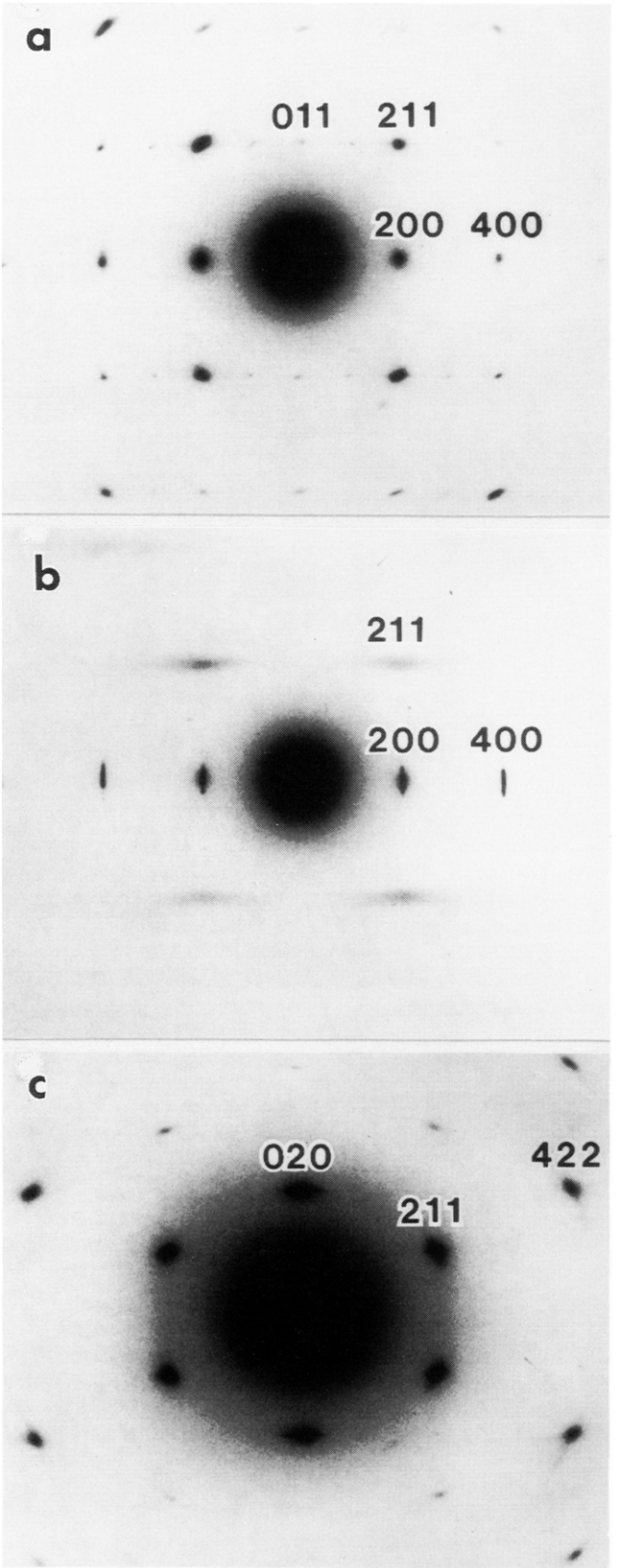

Figure 4. Electron-diffraction patterns of fully syndiotactic polypropylene single crystals (a) crystallized at 140 °C and tilted by 57° about the *a* axis; (b) crystallized at 100 °C and tilted by 57° about the *a* axis; (c) crystallized at 120 °C and tilted by 45° about the *b* axis. The electron beam is directed along [011] in (a) and (b) and along [$\bar{1}$02] in (c).

us to the tentative suggestion[6] of a doubled unit cell along *b*. At higher crystallization temperatures, *e.g.*, 140 °C (Figure 4a), these streaks are now replaced by strong, discrete reflections at a spacing of 0.470 nm, which allow

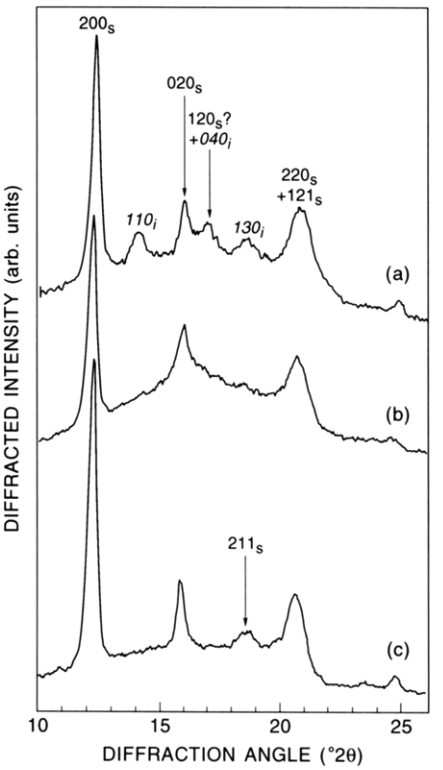

Figure 5. X-ray diffractograms of (a) poorly syndiotactic polypropylene containing 77% racemic triads, typical of all previously studied sPP samples, (b) fully syndiotactic polypropylene as received, and (c) fully syndiotactic polypropylene crystallized isothermally at 135 °C. Subscripts i and s refer to isotactic and syndiotactic polypropylene, respectively.

us to identify them unequivocally as 211 of Cell III. In fact, the reflections in Figure 4a define the *hkk* lattice of an orthorhombic cell with *a* and *c* the same as before but with *b* = 1.120 nm, *i.e.*, *double* its previous value. The same conclusion is reached by tilting about the *b* axis (Figure 4c): A 45° tilt reveals the new 211 spot (and its higher orders, *e.g.*, 422) to be strongly diffracting (the reflecting net here is the 2*l*, *k*, *l*). From the above, we conclude that in *single crystals* of highly syndiotactic polypropylene the preferred packing mode is that of Cell III and therefore that the molecules alternate in hand along *both* the *a* and the *b* axes. This is seen from Figure 4c to be valid at least down to 120 °C. At lower crystallization temperatures, increasing departures from regular antichiral packing occur for kinetic reasons, and these are manifest through the specific streaks observed in both the *hk*0 and other more general reciprocal-lattice layers.

b. Bulk sPP Structure. These results from single crystals of fully syndiotactic polypropylene allow us now to examine directly the structure of *bulk* sPP, whose previous diffraction patterns from less syndioperfrect specimens were complicated by extraneous and unresolved features that had required a number of assumptions for their interpretation.[7,8] Moreover, they allow us also to resolve the previously raised questions about the origins and effects of *isotactic* polypropylene in all earlier specimens.[7,8]

A diffractogram from our previous sPP sample[7] (which contained 77% *rr* triads) is seen in Figure 5 (curve a). The reflections are now identified on the basis of our new, doubled Cell III (which we shall use from now on). The major complexity in this pattern arose from the presence of a reflection at 16.95° 2θ, which would correspond to 120 (or 110 in Cells I and II) and which is permitted *only* by

the original, fully isochiral, Cell I.[4,5] Another complication in this pattern involves the presence of reflections at 14.1° and 18.6° 2θ, which are totally inconsistent with sPP and which we previously attributed[7] to the presence of separate *isotactic* PP sequences that were long enough to crystallize. We should note that, as discussed in ref 7, these unexpected features were in fact present in all previously published X-ray diffractograms that we could find in the literature[2,10-13] (see also Figure 7 of ref 7) but had been interpreted differently: The presence of separate isotactic polypropylene (iPP) reflections was not recognized, the 16.95° peak was assigned to Cell I of sPP, and any isotactic sequences were ascribed to stereoblock defects within the sPP population.

All of these uncertainties and complications are now removed in the diffractogram from the new, fully syndiotactic specimen (curve b in Figure 5). Our attribution of the additional peaks in previous samples to isotactic polypropylene is supported by their absence in this diffractogram. Equally important is the absence of the 16.95° peak whose identification with sPP would be inconsistent with Cells II and III but would require instead packing in the manner of Cell I. As we speculated in ref 7, this peak may arise not from syndiotactic polypropylene but from its isotactic admixture, for which the strong 040 reflection would occur at the observed spacing. Indeed, the absence of this peak in curve b of Figure 5 confirms our original interpretation and validates our alternative packing scheme (Cell II or III). However, the diffractogram of curve b cannot distinguish between these two cells because the specimen had been quickly cooled to room temperature. As a result, the packing defects that we identified in single crystals by the strong streaks in Figures 3 and 4 now contribute to the broad, diffuse background evident in Figure 5b.

However, by prolonged crystallization at high temperature we can reduce this background substantially and strengthen the crystallographic peaks, as seen in curve c of Figure 5. At that point, an additional peak at 18.8° 2θ becomes clearly visible, which we identify as the 211 of Cell III. As we recall from Figure 4 (a and c), this 211 reflection is the strongest one of the series of peaks that necessitate the doubling of the unit cell along b and confirms our fully antichiral packing in sPP. This additional peak could also have been present in our previous, less syndiotactic, specimens but would have been obscured by the 130 of iPP. We should note that this new peak was also recently observed by Galambos *et al.*[14] in a specimen annealed at 150 °C, but its crystallographic nature and structural implications were not discussed.

For a fuller understanding of the chain packing in bulk sPP, we have simulated the powder pattern from Cell III (using the CERIUS Version 3.0 program[15] from Molecular Simulations) and compared it to that from a highly crystalline bulk sPP film (crystallized from the melt at 135 °C and annealed at 10 °C intervals for 10 min during cooling to ambient) from which the amorphous background had been digitally subtracted. These two diffractograms are seen in Figure 6 as curves a and b, respectively. The simulated curve was constructed using Lorentzian peak profiles, crystallographic coherence lengths of 30, 20, and 5 nm along *a*, *b*, *c*, respectively, and an isotropic Debye–Waller temperature factor of 0.031 58 nm^2 corresponding to root-mean-square atomic displacements of 0.02 nm (use of anisotropic factors had negligible effects upon the line shapes at this 2θ range). As seen in Figure 6, there is an excellent match in the fit of the major 200 and 020 peaks. However, the $l \neq 0$ peaks (*i.e.*, the 211, 121, and 002 in this

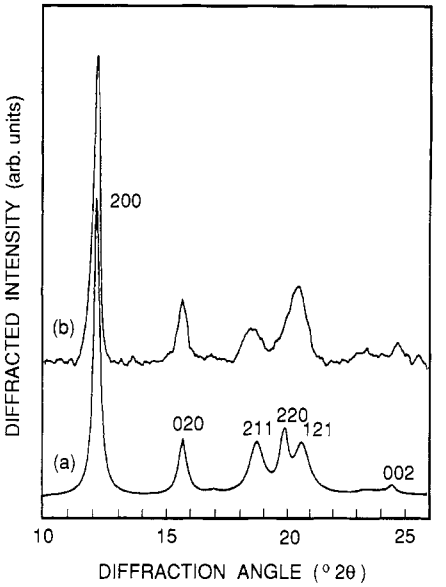

Figure 6. (a) Calculated X-ray diffractogram of fully syndiotactic polypropylene. (b) Experimental diffractogram from sPP crystallized at 135 °C, after subtraction of the amorphous background.

figure) are significantly broadened, with the result that the 220/121 doublet is not resolved in the experimental trace. We attribute the broadening of these reflections to departures along the *c* axis from the exact *Ibca* symmetry implied by Cell III. These departures correspond to *c*-axis packing defects and thus do not affect the *hk*0 reflections; they are discussed immediately below.

c. *c*-Axis Packing Defects. In addition to the *b*-axis packing defects that are evident in *hk*0 patterns from single crystals of sPP, we have discovered in [0$\bar{1}$1] patterns from tilted crystals evidence for additional interchain packing departures along *c*. The evidence centers on the fine features of the *hkk* lattice. As seen in Figure 4a, the *h*11 layer includes a number of weak but unexpected reflections, *i.e.*, the 011, 111, 311, etc. (similar, but weaker reflections are also seen in the *h*22 layer, *e.g.*, 322). Moreover, these reflections are detectable only under very weak electron-irradiation conditions and disappear during observation (at very low doses of *ca.* 20 C/m^2), while the remaining spots remain sharp. To understand the origins of these extra reflections, we simulated the electron-diffraction patterns along the [0$\bar{1}$1] and [001] zones for a crystal of realistic thickness (*ca.* 10 nm, *i.e.*, 13 unit cells along *c*) using the HRTEM module of the CERIUS software package.[15] Briefly, this program simulates electron-diffraction patterns and real-space images by calculating projected potentials and phase-transmission functions as each diffracted beam is propagated through the crystal, using the classic Cowley–Moodie multislicing approximation[16] to the dynamic theory of electron scattering. The projected potentials were calculated from the crystal lattice using fast Fourier transforms for an a* × b* array of 24 × 18 beams.

The simulated [0$\bar{1}$1] pattern from Cell III is seen in Figure 7 together with two unit cell projections showing the (211) and (011) planes, respectively, in edge-on orientations. It is clear that the calculated 211 intensity should be very high (in agreement with our experimental data) but that 011 should be absent. As seen in Figure 7a, the (211) planes contain the planar zigzag $-CH_2CHCH_2-CHCH_2-$ sequences, which contribute a high scattering amplitude. On the other hand, diffraction from the (011) planes is the same as that halfway in-between (see Figure 7b), so that the 011 reflection should be absent.

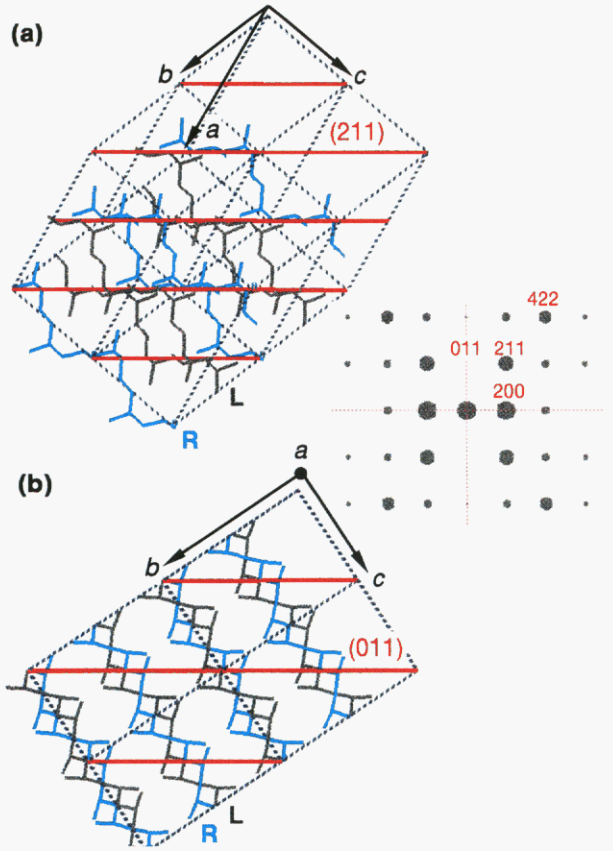

Figure 7. Calculated [0$\bar{1}$1] electron-diffraction pattern for sPP. (a) and (b) show the unit cell projections with the (211) and (011) planes on edge, respectively.

Experimental observation of 011 could have been explained by double diffraction, since its indices can be generated as the sums of the corresponding indices of two primary diffraction spots.[17] However, this is not true for other observed reflections, *i.e.*, *hkk* with $h = 2n + 1$. We therefore considered that the weak but unexpected reflections may arise from *c*-axis packing defects (since their analogues on the *hk*0 layer are absent). We therefore simulated the reciprocal-lattice section along [0$\bar{1}$1] for a number of packings of our fully antichiral Cell III that incorporate small displacements in the chain direction. Figure 8a represents the regular, undeviated packing, while parts b and c of Figure 8 result from displacement of *one* of the four chains in the unit cell by 0.037 or 0.074 nm, respectively (these correspond to 5% and 10% of the length of the *c* axis). As seen in this figure, the additional spots observed experimentally now appear in the simulated electron-diffraction patterns, with intensities for the 10% displacement (Figure 8c) in reasonable agreement. The same holds true for the case of *two* chains per unit cell displaced by 5%, as seen in Figure 8d; other two-chain combinations lead to poorer qualitative agreement. Also, more complex chiral packings (such as RLR, RLRR, RRLL, *etc.*) produce inconsistencies in the *hk*0 and higher layers.

We therefore suggest that one possibility for the extra *hkk* spots may involve small packing departures by *ca.* 5–10% along *c* adopted during crystallization. Such departures need not entail shifts of the entire stem but could instead arise from incorporation of conformational defects. This is consistent with the disappearance of these extra reflections under weak electron irradiation, since mobility of chains is highest along their *c* axes. Such chain motion arises from the high stresses imparted to the molecules by radiation-induced cross-linking of their

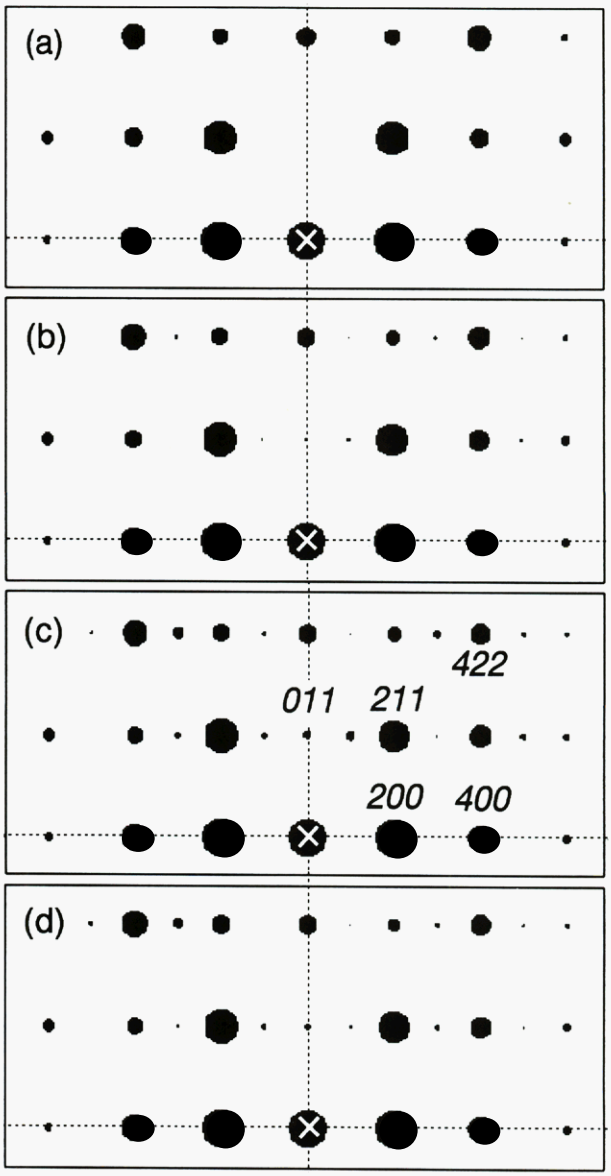

Figure 8. Calculated [0$\bar{1}$1] electron-diffraction patterns for Cell III fully antichiral lattices: (a) regular, undeviated packing; (b) one chain per unit cell displaced by 0.037 nm (*c*/20) along *c*; (c) one chain per unit cell displaced by 0.074 nm (*c*/10); (d) two chains per unit cell at *b*/2 positions displaced by 0.037 nm (*c*/20) along *c* in opposite directions.

amorphous surfaces.[18] Even more severe crystallographic effects involving large-scale changes in both conformation and lateral packing were found in some polymers, *e.g.*, poly(vinylidene fluoride), under irradiation.[19,20]

d. Simulation of *b*-Axis Packing Defects. As we showed in section a, the prominent streaks in the *hk*0 diffraction patterns (Figure 3) clearly arise from a packing defect along the *b* axis corresponding to occasional *C*-centered (isochiral) placement of sPP chains. However, the precise nature, propagation, and extent of these defects is still not known. For this reason, we have simulated a number of different possibilities using two complementary techniques, *i.e.*, optical diffraction and molecular modeling. Optical diffraction has the advantages that (a) very large lattices can be simulated, (b) a variety of complicated, nonperiodic defects can be simultaneously incorporated, and (c) the diffraction patterns can be obtained simply and rapidly. Its disadvantage lies in the fact that the precise bond structure and atomic scattering of the individual molecules are not explicity accounted for, since a simplified projection of the chains is taken along the

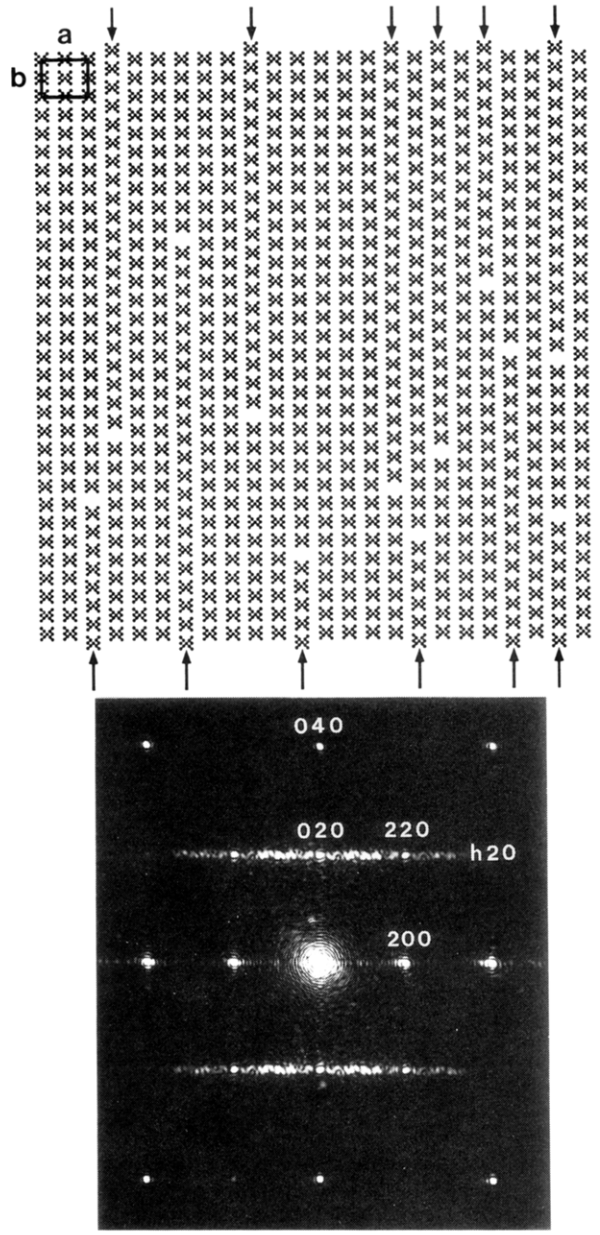

Figure 9. Simplified model sPP lattice in a [001] projection incorporating $b/4$ point vacancies that are allowed to spread to the edge of the crystal (arrows) and its corresponding optical diffraction pattern.

incident-beam direction. Computer modeling, on the other hand, rigorously preserves the fine details of the chain structure and atomic scattering contributions but is restricted as to the size of crystal and complexity of defects that its working memory can accommodate.

For optical diffraction, photographically reduced masks of $hk0$ crystal projections containing various packing defects were illuminated by a He–Ne laser on an optical bench. The masks were drawn on a computer using disks to represent the [001] projections of the methyl, methylene, and methine groups in their appropriate positions within the sPP lattice. This technique yields optically the power spectrum of the two-dimensional Fourier transform of the lattice, as described in great detail by Tanaka *et al.*[21]

The type of defect modeled is a $b/4$ vacancy at the point where an isochiral chain placement (Cell I packing) might be introduced within a Cell III crystal lattice. Other fractions of the b axial length would also lead to the observed streaking but are not considered here for steric reasons (low-energy packings in any of the proposed unit

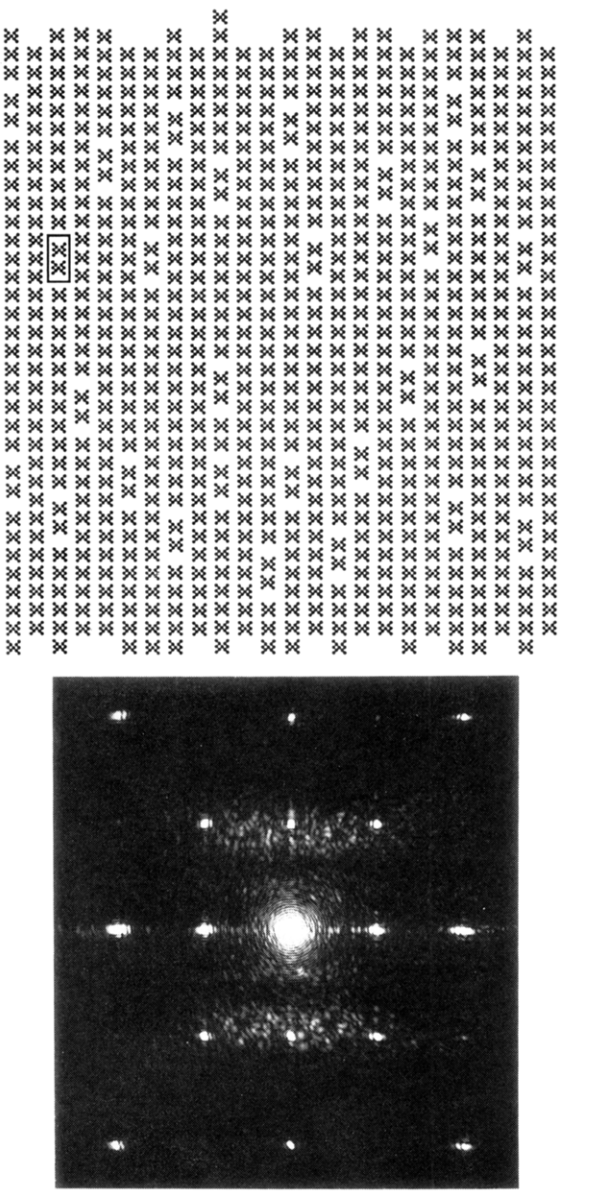

Figure 10. Simplified model sPP lattice in a [001] projection incorporating $b/4$ point vacancies that are allowed to spread along b to only one adjacent chain.

cells all involve chains at $b/4$ positions or at its multiples). For the same reasons we also do not consider random packing of chains in the regular Cell III positions but without regard to their chirality: Isochiral packing in a Cell III lattice is sterically unfavorable (see also the schematic of Figure 2).

The first defective lattice that we model is seen in Figure 9 together with its optical diffraction pattern. Here we examine the case where a $b/4$ defect, once introduced, will propagate along b to the edge of the crystal in a localized Cell I packing (see arrows in Figure 9), since otherwise a second such defect would have to be nucleated to revert to the dominant Cell III packing. Thus, in the example modeled in Figure 9, the 12 defects nucleated within the lattice lead to 50% Cell I (isochiral) packing. When we compare the resulting optical diffraction pattern with actual experimental ones (*e.g.*, Figure 3), we find agreement in the general features, *i.e.*, sharp $hk0$ reflections for even values of h or k (and absence for odd) and a pronounced streak along $h20$. However, the fine characteristics of this streak are not consistent with our experimental evidence: the streak is too intense and too broad compared to the discrete spots. This is, of course, a result of the high

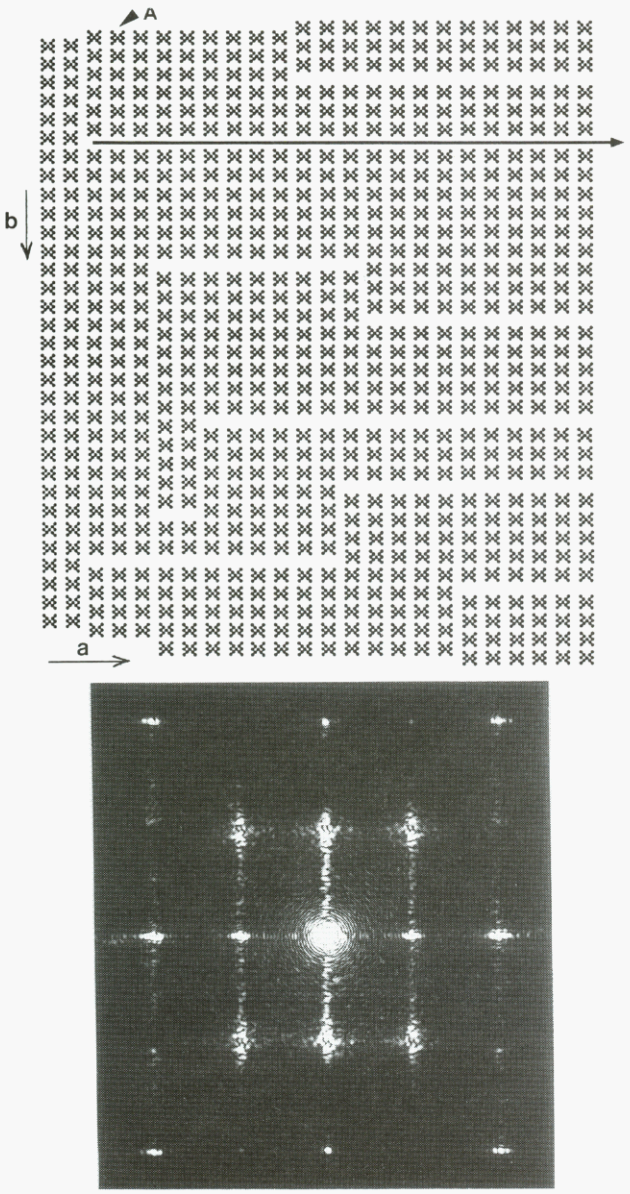

Figure 11. Simplified model sPP lattice in a [001] projection incorporating $b/4$ point vacancies that are mutually aligned to yield row vacancies along a and its corresponding optical diffraction pattern.

proportion of Cell I packing coupled with the presence of numerous $b/4$ vacancies.

A slightly different model is simulated in Figure 10. Here, we probe the case where the probability for nucleation of isochiral defects is high, but their propagation along b is limited. This assumes that the Cell I packing is energetically less favorable than its antichiral counterparts and is modeled here for the extreme case where the defective packing along b is limited to only two chains. As seen in the corresponding optical diffractogram, this causes the diffue $h20$ streak to be extremely broadened along b^* (as would be expected from the small extent of the defect and the large number of $b/4$ vacancies) and demonstrates that this is not actually encountered in sPP. We therefore infer that the energetics of b-axis propagation of the two possible packings must be very close and that the rarity of the Cell I packing must be attributed to low nucleation probability.

If the spreading rate of the defective packing along b is high, is there any persistence along a? The reason that this is to be considered has to do with the relative energetic

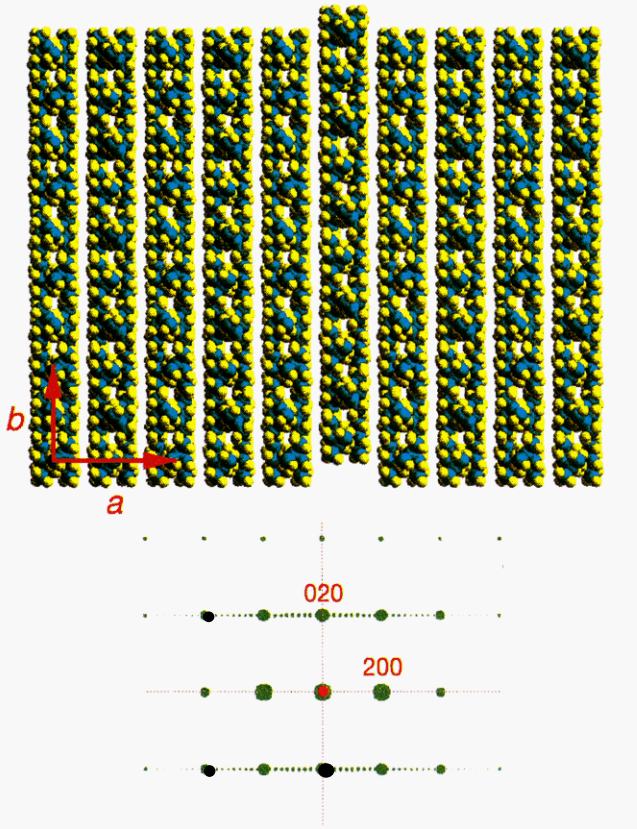

Figure 12. Computer-generated Cell III sPP lattice in a [001] projection incorporating a single full row of molecules displaced by $b/4$ and its corresponding calculated $hk0$ electron-diffraction pattern.

costs of bridging an underlying $b/4$ gap on the substrate *vs* propagating this defect. As seen in the simulated lattice of Figure 11, when a chain (A in this figure) begins to deposit in the dominant antichiral manner on top of a bc substrate containing such a gap, it will eventually be faced with a choice: either to bridge the $b/4$ gap on the substrate and thus be forced into a Cell I (isochiral) mode (both of which would be energetically costly) or simply to continue its antichiral packing by following the topography of the substrate and thus propagate the gap. This would result in $b/4$ row vacancies aligned along a (arrow in Figure 11). However, the diffraction pattern in Figure 11 demonstrates that the incoherent mutual arrangements of these vacant rows would cause pronounced streaks along a^*, which are certainly absent in all experimental sPP patterns; therefore, any extended row vacancies must be rejected.

From all of the above simulation results, we conclude that *appreciable* presence of vacancies *of any type* would cause unacceptable broadening or additional artifacts to the $hk0$ streaks. We thus infer that such vacancies may preferentially be rejected to the crystal periphery. Since these vacancies represent *fractional* molecular widths along b, they cannot be rejected to the lateral sides of the crystal (*i.e.*, by movement of molecules along a). They could only be rejected along the crystal growth direction (*i.e.*, b). This means that the vacancies must either travel to the growth front and be annihilated there during the actual crystallization or else travel backward (or forward) within the crystal until they can aggregate adjacently to yield a macroscopic row defect. Such a row defect will then constitute a *fault* in the ac plane, which should favor localization of transverse crystal fracture. Such transverse fracture is documented in our morphological study[9] of fully syndiotactic PP, where we also provide evidence for

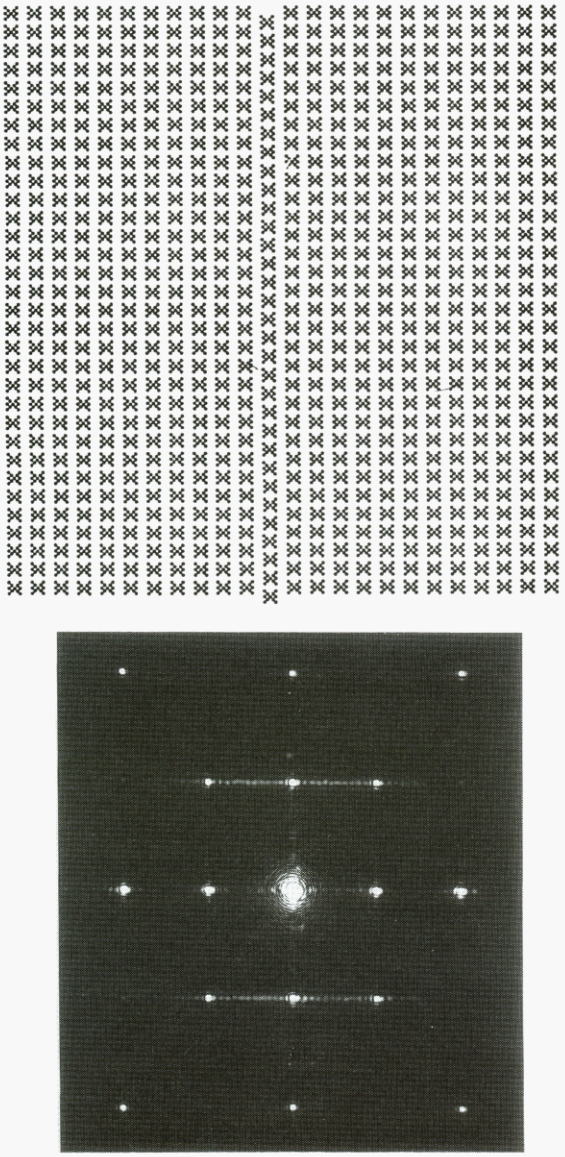

Figure 13. Same as Figure 12 but for a much larger and simplified lattice probed by optical diffraction.

a much higher thermal expansion coefficient along the b axis than along the a (17.93×10^{-4} *vs* 2.39×10^{-4}, respectively). We also show in that study[9] that, based upon decoration with evaporated polyethylene,[22] the folds are preferentially disposed *toward the growth direction* (*i.e.*, along the b axis) in many crystalline regions. This is a most unusual phenomenon and has obvious implications on the manner in which adjacent stems might adopt antichiral arrangements; these questions will be discussed in detail in our morphological study.[9]

In simulating lattices where the vacancies have been pushed to the crystal edge (*i.e.*, where entire rows of molecules have been displaced by $b/4$, we used computer modeling since lattice size requirements do not need to be as large as in the previous cases. This offers the advantages of incorporating rigorously the individual geometrical and scattering parameters for each atom in the lattice, as well as probing realistically thick crystals (with consequent dynamical effects). An example of the calculated [001] electron-diffraction pattern for a crystal of 10×10 chains with a single row displaced along b is seen in Figure 12 using once again the CERIUS program (in this and the following computer-modeled lattices, the atoms are shown at 70% of their van der Waals radii for better visual distinction of the individual chains). The calculated

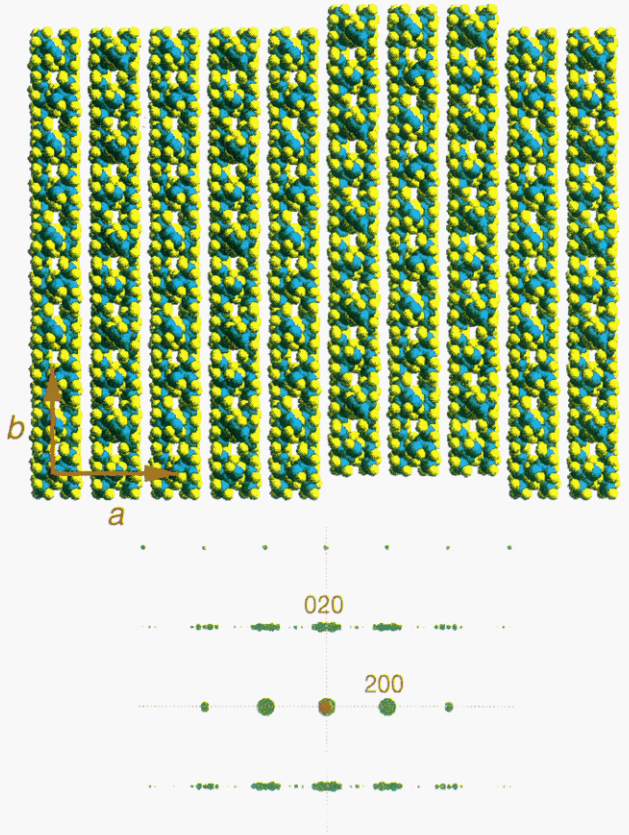

Figure 14. Computer-generated Cell III sPP lattice in a [001] projection incorporating domains of molecular rows displaced by $b/4$ and its corresponding calculated $hk0$ electron-diffraction pattern.

pattern now seems to be in excellent agreement with experimental patterns from crystals grown at high temperatures (>120 °C as seen in Figure 3a-c). In particular, we should pay attention to the sharpness of the discrete $h20$ spots and the narrowness of the superposed streak in the simulated pattern of Figure 12 (here, of course, the "streak" consists of discrete spots because of the small size of the lattice). This is to be distinguished from the unrealistically broadened streak of Figure 9, for which vacancies were incorporated *within* the simulated crystal. For a direct comparison between these two alternatives, the reader may examine the optical diffractograms of Figures 9 and 13. The latter arises from a much larger lattice than in Figure 12 (containing 24×32 "molecules", with one displaced central row). Also, comparison of the optical and computer-calculated diffraction patterns (Figures 13 and 12, respectively) demonstrates the validity of simplifying the chain structure into an assembly of disks representing methyl, methylene, and methine groups when constructing the simulated lattice for optical diffraction.

From the above, we conclude that the defective packing in sPP *at high temperatures* consists of occasional displacement by $b/4$ of essentially full rows of molecules. Such defects are indeed very rare: comparing the relative intensities of $h20$ streaks *vs* discrete spots in experimental and simulated patterns, we estimate that fewer than 1 in 30 rows is displaced at high temperatures. But, what is the nature of the defect at lower crystallization temperatures (*i.e.*, <120 °C) where, in addition to the streak, the discrete $h20$ reflections are *themselves* markedly elongated? (See Figure 3c-e.) Elongation of individual reflections along a^* at a constant b^* value implies that *groups* of rows (rather than individual rows) are now displaced by $b/4$. An example of this is seen in Figure 14,

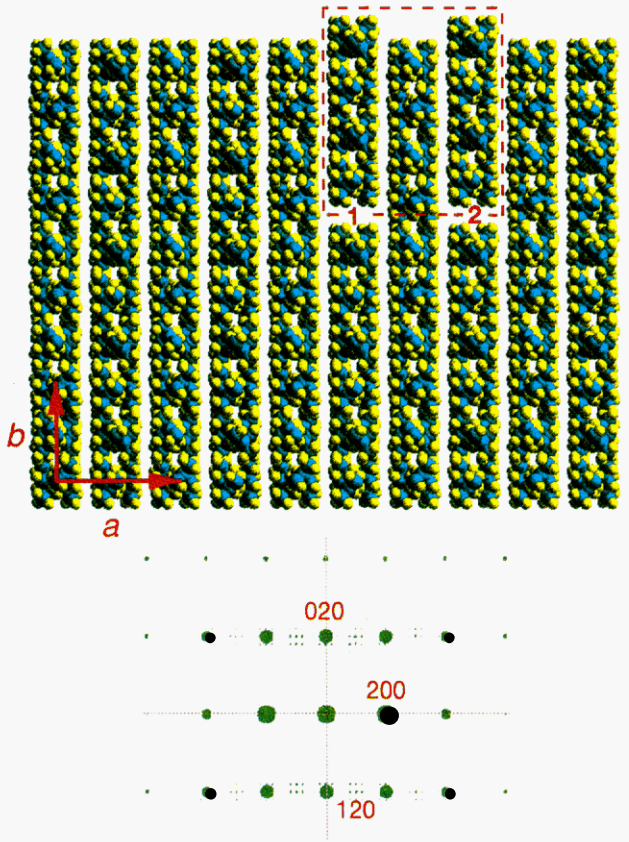

Figure 15. Computer-generated Cell III sPP lattice in a [001] projection incorporating mutually registered $b/4$ displacements in rows 1 and 2 and its corresponding calculated $hk0$ electron-diffraction pattern.

where the same 10 × 10 lattice of Figure 12 now contains three adjacent rows displaced *as a group*. Even though the streaks in both of these simulated patterns consist of individual spots rather than of continuous scattering (this is obviously a result of the smallness of the artificial lattice), their close correspondence to the experimental evidence is remarkable. We therefore conclude that, as the crystallization temperature is lowered, the crystals consist increasingly of *domains* of antichiral chains that are mutually displaced by $b/4$. The boundaries between these blocks correspond to half of Cell I and probably represent facile slip planes. The increasing frequency of formation of such mutally displaced domains with diminishing crystallization temperature can be attributed to kinetic reasons.

The last question that we address is the following: Since the domain walls are in essence half-cells of Type I (isochiral), does their proliferation at lower growth temperatures also favor their mutual aggregation into discrete islands of Cell I structure? Our evidence from fully syndiotactic polypropylene argues against that. We have simulated such an island in Figure 15, keeping its dimensions deliberately small by displacing only parts of rows 1 and 2. Nevertheless, as seen from the accompanying diffraction pattern, there should be distinguishable intensity maxima at the 120 positions. In fact, even for a Cell I island as small as 4% we can observe clear 120 reflections within a simulated lattice (this is seen in Figure 16, for which we have used the optical technique in order to be able to incorporate such a minute amount of defective packing). When we now compare these simulated findings with our experimental data (*e.g.*, Figure 3c-e, and many others), we observe no correspondence: the intensity maxima on the $h20$ layer occur only at $h = 2n$ positions.

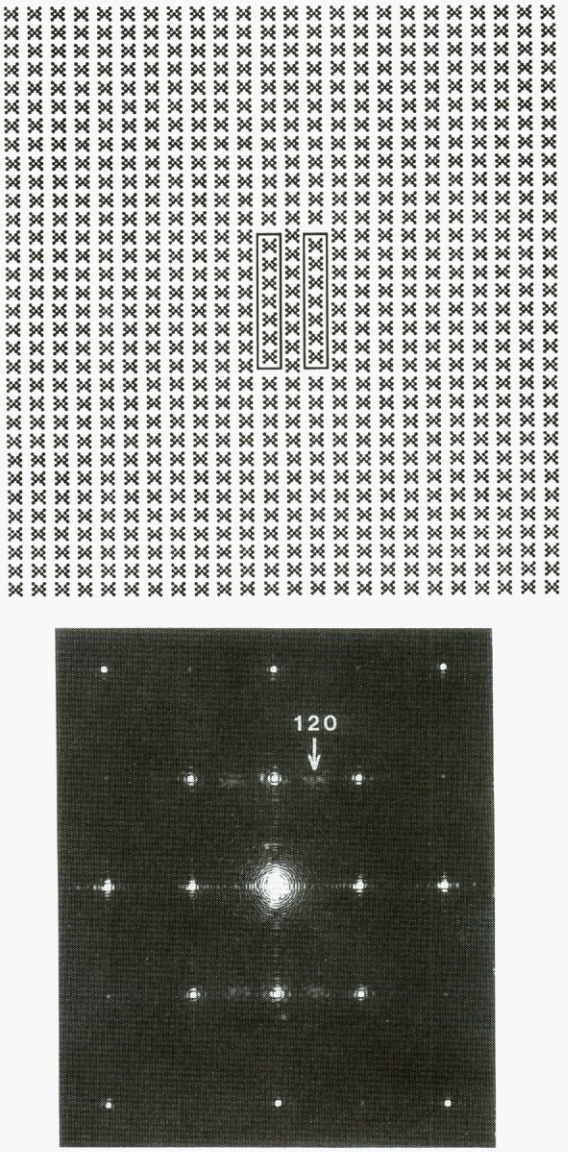

Figure 16. Same as Figure 15 but for a larger and simplified Cell III lattice incorporating a very small (3.9%) amount of a Cell I defect.

On the other hand, there is some evidence for very limited Cell I defects in less syndioregular sPP. In our previous samples (containing *ca.* 77% racemic triads) we did identify weak, diffuse 120 intensity peaks within the $h20$ streak at low crystallization temperatures (see, *e.g.*, Figure 1c-f of ref 8). Even there, however, the $h = 2n$ maxima were much stronger, so that the isochiral islands occurred only as rare packing defects.

Conclusions

By conducting this first structural investigation of essentially 100% syndiotactic polypropylene, we established that the stable, high-temperature, unit cell comprises fully antichiral packing along *both* the a and the b axes and is therefore doubled from its widely accepted dimensions. This confirms our earlier suggestion[6] from less syndioperfect (76%) specimens. The unit cell is thus orthorhombic with $a = 1.450$ nm, $b = 1.120$ nm, $c = 0.740$ nm, and space group *Ibca*. Such fully regular antichiral packing is obtained only at the highest crystallization temperatures (*i.e.*, ≥130 °C), with progressive incorporation of isochiral packing defects as the temperature is lowered. We examined a large number of potential packing defects using molecular modeling and optical diffraction

and rejected any large-scale occurrence of point or row vacancies. Instead, we conclude that point vacancies (where isochiral defects are initiated) may be rejected to growth fronts or aggregate within the crystal, where they may localize initiation of transverse faults. The defective packing then corresponds to either (a) extended rows of molecules displaced by $b/4$ or (b) groups of such molecular rows displaced by $b/4$ to yield discrete domains. The first is observed at high temperatures and is identified by weak, continuous streaks superimposed on sharp $h20$ spots. The second, identified by elongated $h20$ reflections, occurs increasingly at lower crystallization temperatures. Islands of isochiral packing defects could not be identified in our fully syndiotactic polypropylene specimens but were present in very limited extent in previous, less syndioregular samples grown at low temperatures. Finally, by modeling the *hkk* layer of the reciprocal lattice and comparing it to diffraction patterns from tilted single crystals, we discovered an additional packing defect in sPP, this one along the molecular axis. The structure appears to involve displacement of one or two chains (or parts of chains) per cell by 5–10% of the length of the c-axis repeat and may be related to conformational defects within the molecules.

Acknowledgment. We are very grateful to Dr. T. Simonazzi of Himont Research Center, Novara, Italy, for provision of the fully syndiotactic specimen, to Professor D. C. Martin of The University of Michigan for a helpful suggestion on domain walls, and to our colleague Dr. P. A. Mirau for NMR determination of the syndiotacticity of our specimen.

References and Notes

(1) Permanent address: Institut Charles Sadron, CNRS-ULP, Strasbourg, France.
(2) Boor, J., Jr.; Youngman, E. A. *J. Polym. Sci., Polym. Chem. Ed.* **1966**, *4*, 1861.
(3) Ewen, J. A.; Jones, R. L.; Razavi, A.; Ferrara, J. D. *J. Am. Chem. Soc.* **1988**, *110*, 6255.
(4) Natta, G.; Pasquon, I.; Corradini, P.; Peraldo, M.; Pegoraro, M.; Zambelli, A. *Atti. Acc. Naz. Lincei* **1960**, *28*, 539.
(5) Corradini, P.; Natta, G.; Ganis, P.; Temussi, P. A. *J. Polym. Sci. Part C* **1967**, *16*, 2477.
(6) Lotz, B.; Lovinger, A. J.; Cais, R. E. *Macromolecules* **1988**, *21*, 2375.
(7) Lovinger, A. J.; Lotz, B.; Davis, D. D. *Polymer* **1990**, *31*, 2253.
(8) Lovinger, A. J.; Davis, D. D.; Lotz, B. *Macromolecules* **1991**, *24*, 552.
(9) Lovinger, A. J.; Lotz, B.; Davis, D. D. *Macromolecules*, to be submitted.
(10) Natta, G.; Pasquon, I.; Zambelli, A. *J. Am. Chem. Soc.* **1962**, *64*, 1488.
(11) Zambelli, A.; Natta, G.; Pasquon, I. *J. Polym. Sci., Part C* **1963**, *4*, 411.
(12) Inagaki, H.; Miyamoto, T.; Ohta, S. *J. Phys. Chem.* **1966**, *70*, 3420.
(13) Ogawa, T.; Elias, H.-G. *J. Macromol. Sci., Chem.* **1982**, *A17*, 727.
(14) Galambos, A. F.; Wolkowicz, M.; Zeigler, R.; Galimberti, M. *Polym. Mater. Sci. Eng.* **1991**, *64*, 45.
(15) CERIUS Version 3.0 Release Notes, 1992, Molecular Simulations, Cambridge, U.K.
(16) Cowley, J. M.; Moodie, A. F. *Acta Crystallogr.* **1957**, *10*, 609.
(17) Hirsch, P.; Howie, A.; Nicholson, R. B.; Pashley, D. W.; Whelan, M. J. *Electron Microscopy of Thin Crystals*; Krieger: Malabar, FL, 1977.
(18) Ungar, G.; Keller, A. *Radiation Effects in Polymers*; Clough, R. L., Shalaby, S. W., Eds.; ACS Symposium Series 475; American Chemical Society: Washington, DC, 1991; Chapter 7.
(19) Lovinger, A. J. *Macromolecules* **1985**, *18*, 910.
(20) Lovinger, A. J. *Radiation Effects in Polymers*; Clough, R. L., Shalaby, S. W., Eds.; ACS Symposium Series 475; American Chemical Society: Washington, DC, 1991; Chapter 6.
(21) Tanaka, H.; Hayashi, T.; Nishi, T. *J. Appl. Phys.* **1986**, *59*, 3627.
(22) Wittmann, J. C.; Lotz, B. *J. Polym. Sci., Polym. Phys. Ed.* **1985**, *23*, 205.